Multifunctional Nanoparticles

DOI: 10.1002/anie.200800857

Drug-Loaded Superparamagnetic Iron Oxide Nanoparticles for Combined Cancer Imaging and Therapy In Vivo**

*Mi Kyung Yu, Yong Yeon Jeong, Jinho Park, Sangjin Park, Jin Woong Kim, Jung Jun Min, Kyuwon Kim, and Sangyong Jon**

Cancer treatments using metallic or inorganic nanoparticles are attracting increased attention because of their novel, intrinsic physical properties and their abilities to target specific locations, thereby minimizing severe side effects.[1–3] In particular, the potential of magnetic nanoparticles in drug delivery has been investigated.[4] Very recently, anti-HER2, antibody-conjugated, multifunctional magnetopolymeric nanohybrids have demonstrated their potential use in simultaneous breast cancer imaging and therapy in vivo.[5] The main advantages of magnetic nanoparticles are that they can be 1) visualized by magnetic resonance (MR) imaging; 2) guided to target sites by means of an external magnetic field; 3) heated to provide hyperthermia for cancer therapy; and 4) degraded into nontoxic iron ions in vivo. A major issue with the current metallic or inorganic nanoparticles that have shown great potential in imaging and therapy is the high risk of toxicity associated with their long-term residence in body without degradation. In light of this issue, the biodegradability of superparamagnetic iron oxide nanoparticles (SPIONs) is highly beneficial for in vivo applications.[6] Therefore, anticancer drugs such as epidoxorubicin- and mitoxantrone-bound magnetic fluids have been developed and used for locoregional cancer treatment in phase I clinical trials.[7] However, these systems have turned out to be effective only under the appropriate strength of the external magnetic field that is necessary to control the residence time of the nanoparticles in the desired area.

[*] M. K. Yu, J. Park, S. Park, Prof. S. Jon
Research Center for Biomolecular Nanotechnology
Department of Life Science
Gwangju Institute of Science and Technology (GIST)
1 Oryong-dong, Buk-gu, Gwangju 500-712 (South Korea)
Fax: (+82) 62-970-2504
E-mail: syjon@gist.ac.kr
Homepage: http://life.gist.ac.kr/nmbm

Prof. Y. Y. Jeong, Prof. J. W. Kim, Prof. J. J. Min
Department of Radiology
Chonnam National University Medical School
Gwangju 501-746 (South Korea)
Fax: (+82) 61-379-7133

Prof. K. Kim
Department of Chemistry, University of Incheon (South Korea)

[**] This work was supported by grants from the National R&D Program for Cancer Control, Ministry of Health and Welfare, Republic of Korea (S.J., M.Y., J.P., and Y.J.; 0720210 and 0520080-1). We also thank Prof. B. K. Cho at GIST for the magnetization measurement.

Supporting information for this article is available on the WWW under http://dx.doi.org/10.1002/anie.200800857.

Very recently, our group reported anti-biofouling polymer coated, thermally cross-linked superparamagnetic iron oxide nanoparticles (TCL-SPIONs) as a novel MR contrast agent for in vivo cancer imaging,[8] and Cy5.5-conjugated TCL-SPION as a dual (MR/optical) cancer-imaging probe.[9] Although TCL-SPIONs do not possess any targeting ligands on their surfaces, the stable and anti-biofouling polymer coating layers allow them to accumulate in tumors by the enhanced permeability and retention (EPR) effect,[10] resulting in efficient tumor detection in vivo. Encouraged by the ability of TCL-SPION to accumulate in tumors, we expected that TCL-SPION could deliver anticancer drugs to tumor sites with high efficiency. Herein we report a novel strategy for combined cancer imaging and therapy by employing TCL-SPION as a drug-delivery carrier. In the current study, we produced and characterized doxorubicin-loaded (Dox; an anticancer drug) TCL-SPION (referred to as Dox@TCL-SPION) as a novel drug-delivering MR contrast agent. Furthermore, its ability to detect tumor, its antitumor efficacy, and its systemic toxicity were evaluated on animal models.

The preparation of Dox@TCL-SPION is shown schematically in Figure 1a. TCL-SPIONs bearing carboxyl groups in the polymer coating layers were synthesized as described previously.[9] We hypothesized that Dox could be incorporated in the polymeric shell of TCL-SPION through electrostatic interactions between positively charged Dox and the negatively charged polymer coating layers.[11] To examine whether such a binding phenomenon occurs, we carried out binding studies as reported previously.[12] We monitored the fluorescence change of Dox upon addition of increasing amounts of TCL-SPION dispersed in 5% glucose solution. The fluorescence of Dox is quenched when the compound is adsorbed onto nanoparticles as a result of electronic energy transfer.[13] Sequential decreases in the intensity of native fluorescence spectrum of Dox were observed as increasing amounts of TCL-SPION were added (Figure 1b). The maximal quenching of Dox fluorescence was achieved with approximately 4 μg of Dox to 200 μg of TCL-SPION, indicating that the optimal loading amount of Dox to TCL-SPION is about 2 wt%.

Dox@TCL-SPIONs were characterized by various measurement methods: particle size, surface charge, and magnetization. Electrophoretic light scattering (ELS) and transmission electron microscopy (TEM) measurements revealed that the incorporation of Dox to TCL-SPIONs did not affect their size (Figure 2a and Supporting Information). Dox@TCL-SPION showed a mean hydrodynamic size of 21 ± 6 nm and a narrow size distribution (PDI = 0.13). The appreciable decrease in the zeta-potential of Dox@TCL-SPION ($-25 \pm$

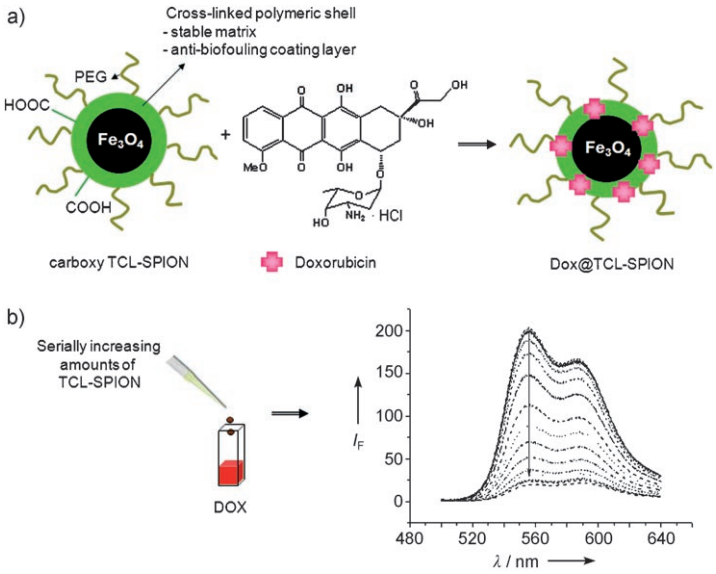

Figure 1. a) Formation of Dox@TCL-SPIONs. b) Fluorescence spectra of Dox solution (4 μg in 150 μL of 5% glucose solution) with increasing amounts of TCL-SPION (from top to bottom: 0.18, 0.37, 0.75, 1.5, 3, 6.25, 12.5, 25, 50, 70, 100, 130, 150, 180, 200, 220, and 250 μg).

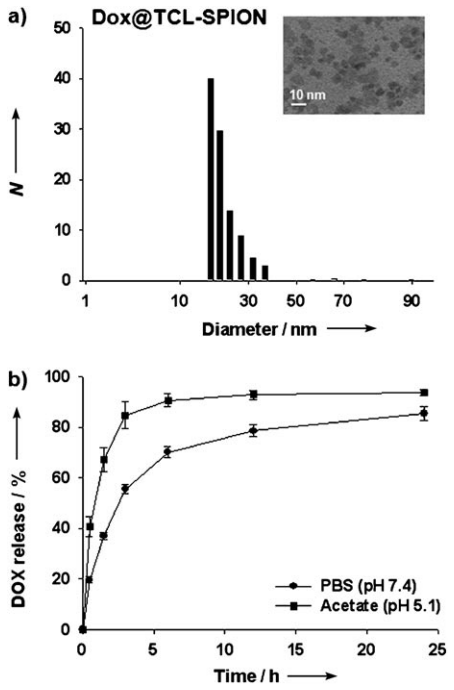

Figure 2. a) Hydrodynamic size distribution and TEM image of Dox@TCL-SPIONs. b) Drug-release profiles for Dox@TCL-SPION measured at pH 5.1 in acetate buffer and at pH 7.4 in PBS buffer (average of three measurements).

2 mV) relative to that of TCL-SPION (-37 ± 2 mV) is evidence that some negatively charged carboxylate groups on TCL-SPION were neutralized by the positively charged drug. As expected, Dox@TCL-SPION exhibited superparamagnetic behavior with a saturation magnetization (M_S) of approximately 70 emu g^{-1} (see the Supporting Information).

The drug-release kinetics for Dox@TCL-SPION were studied by using a dialysis bag at two different pH conditions (Figure 2b; see Supporting Information for experimental details). We assumed that Dox release would be faster at mildly acidic pH values than at neutral pH as a consequence of weakened binding between Dox and the partially neutralized carboxy groups in TCL-SPION. As expected, upon dialysis, approximately 60% of the drug was released within 50 min at pH 5.1 in acetate buffer, whereas at pH 7.4 in PBS buffer, it took 4 h to attain a comparable level of drug release. These data imply that the physically bound drug molecules could be released faster in the mild acidic environments of tumor areas than at the physiologically neutral pH of blood in the vascular compartment.

We next examined whether Dox@TCL-SPIONs are still able to localize and accumulate in tumors by EPR effect as TCL-SPIONs did.[8,9] Tumor-bearing mice were prepared by subcutaneous injection of Lewis lung carcinoma (LLC) cells into the right back of mice, and then MR imaging of the mice was performed at scheduled time points after the intravenous injection of Dox@TCL-SPION (4 μg of Dox, 500 μg of TCL-SPION) in 5% glucose solution. Previously, we found that the use of 5% glucose solution instead of PBS buffer for TCL-SPION injection could diminish the accumulation in the liver and lungs, which are well known filters for nanoparticles.[9,14] Before injection of Dox@TCL-SPION, the tumor appears as a hyperintense area in T_2-weighted MR images (white arrow and dashed circle in Figure 3a). The relative signal enhancement (RSE, %) was calculated in the region of interests (ROIs) of the T_2-weighted images. At 4.5 h postinjection, noticeable darkening appeared in the tumor area with a RSE value of about 58%, indicating a large accumulation of the nanoparticles within the tumor. The RSE measurements revealed maximum localization of the nanoparticles at the ROIs (t_{max}) after between 4.5 and 12 h postinjection, and most of the nanoparticles were removed from the tumor within 24 h (see the Supporting Information).

To examine the distribution of Dox in mice, we obtained ex vivo fluorescence images of several major organs after intravenous injection of both free Dox and Dox@TCL-SPION at similar time points as the MR measurements (Figure 3b and c). The pseudocolor-adjusted images showed a relatively intense fluorescence signal exclusively in the tumor areas even 1 h after injection of Dox@TCL-SPION, which is indicative of the fast accumulation and the release of Dox within the tumor area. The maximum fluorescence intensity was observed in the tumor at 12 h postinjection, indicating the t_{max} of Dox (see the Supporting Information). In contrast, when free Dox was injected into mice as a control, there was no considerable difference between tumor and other organs, and much lower intensity relative to the cases of the drug-loaded nanoparticles. This finding suggests that Dox was delivered to the tumor site by the TCL-SPIONs, and then released from the nanoparticles. Furthermore, the fluorescence intensities in the liver were very weak in the cases of Dox@TCL-SPION injected mice at all time points relative to

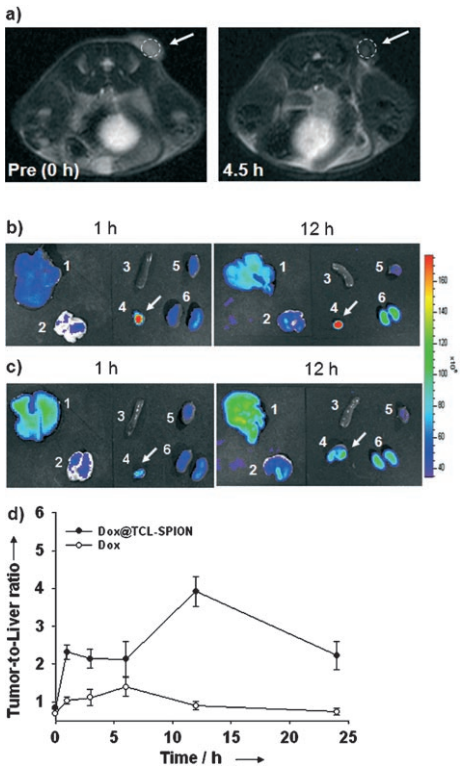

Figure 3. a) T_2-weighted fast-spin echo images (time of repetition/time of echo: 4200 ms/102 ms) taken at 0 h and 4.5 h after injection of Dox@TCL-SPION at the level of LLC tumor on the right back of the mouse. The dashed circle with white arrow indicates the allograft tumor region. b,c) Optical fluorescence images of major organs and allograft tumors: 1 liver; 2 lung; 3 spleen; 4 tumor; 5 heart; 6 kidney. Images were taken after intravenous injection of b) Dox@TCL-SPION (equivalent to 4 μg of Dox) and c) free Dox (4 μg) into tumor-bearing mice ($n=3$), mice were euthanized after 1 h and 12 h. d) The ratio of fluorescence intensities of tumor to liver for Dox@TCL-SPION (closed circles) and free Dox (open circles) as a function of time.

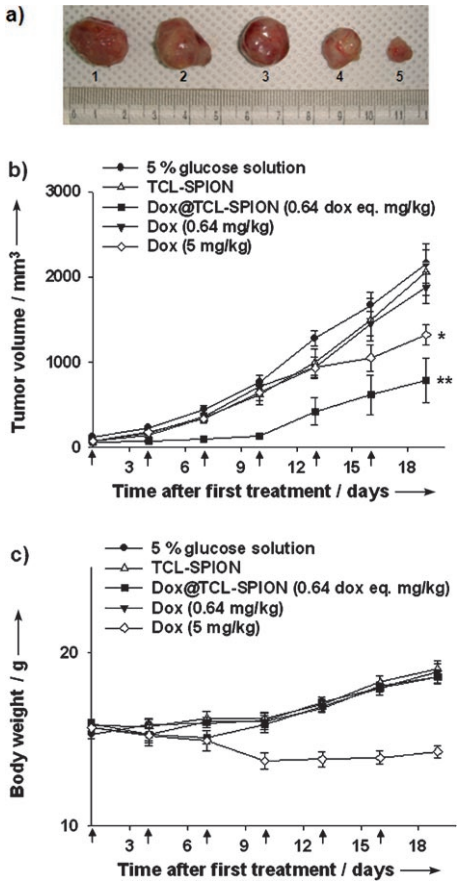

Figure 4. Antitumor efficacy of Dox@TCL-SPION in LLC allograft animal model. a) Excised tumors from mice euthanized after the 19th day of treatment with: 1 control; 2 TCL-SPION (12.5 mg Fe kg^{-1}); 3 Dox (0.64 mg kg^{-1}); 4 Dox (5 mg kg^{-1}); 5 Dox@TCL-SPION (12.5 mg Fe kg^{-1}, 0.64 mg Dox kg^{-1}). b) Tumor volume inhibition results from each treatment group (*$P<0.005$, **$P<0.01$, $n=5$–7). c) Evolution of body weight of each group during the treatment. Arrows indicate the day of drug injection.

the cases of free Dox injected mice (Figure 3 b–d), implying that much lower organ toxicity would be anticipated with TCL-SPION-based drug-delivery vehicles. The ratio of fluorescence intensity of tumor to liver over time (Figure 3 d) clearly indicates the benefit of Dox@TCL-SPION compared with free Dox: for example, the highest uptake in target tumor site and the lowest uptake in nontarget liver site was observed at 12 h post injection with around fourfold higher tumor/liver ratio than that of free Dox. In other words, the therapeutic efficacy could be maximized while minimizing unwanted side effects such as toxicity to other organs.

To validate the therapeutic efficacy of Dox@TCL-SPION, we randomly sorted mice bearing established LLC cells into five groups ($n=5$-7) and treated each group with one of following reagents: 5% glucose solution as a control; TCL-SPION (12.5 mg Fe kg^{-1}); Dox@TCL-SPION (12.5 mg Fe kg^{-1} and 0.64 mg Dox kg^{-1}); Dox (0.64 mg kg^{-1}); Dox (5 mg kg^{-1}). As shown in Figure 4 a and b, the Dox@TCL-SPION group showed remarkable inhibition of tumor growth of approximately 63% relative to the control, unlike other groups, such as 5% glucose, TCL-SPION, and Dox (0.64 mg kg^{-1}). The highest dose group of free Dox (5 mg kg^{-1}) showed tumor growth inhibition effects of around 38%; however, despite the eightfold higher dose than the Dox@TCL-SPION group, it exhibited much lower antitumor activity than the latter, whereas its apparent toxicity was more significant as seen in the reduction of body weight (Figure 4 c). Consistent with previous MR imaging and Dox distribution results, Dox@TCL-SPION largely localized in tumors and thus resulted in superior therapeutic outcome to the equivalent dose of Dox group (0.64 mg kg^{-1}) or even the much higher dose of Dox (5 mg kg^{-1}). These results indicate that Dox@TCL-SPION can efficiently reach the tumor sites and then release drugs without any help from magnetic fields or from targeting ligands such as monoclonal antibodies and peptides, which may be attributed to the high stability and the anti-biofouling characteristics of the novel polymer shell in TCL-SPION.

To examine sub-acute toxicity, we measured organ weights from normal mice at 3 days after the last injection of one of following reagents: 5% glucose solution as a control; Dox@TCL-SPION (12.5 mg Fe kg^{-1} and 0.64 mg

Dox kg^{-1}); Dox (5 mg kg^{-1}). Dox@TCL-SPION caused no toxicity in the major organs (see the Supporting Information), whereas the Dox group showed severe toxicity in the liver and spleen, which may have risen from hepatic impairment and lymphatic damage, respectively.[15] In addition, analysis of white blood cell (WBC) counts demonstrated that the treatment with Dox@TCL-SPION was nontoxic, whereas the Dox group showed significantly decreased WBC count relative to the control group, indicating direct cytotoxic myelosuppresion in mice (see the Supporting Information). These results clearly indicated that rationally engineered TCL-SPIONs can be used as efficient drug carriers while minimizing undesirable side effects encountered in current chemotherapy.

In conclusion, the excellent passive tumor targeting efficiency of TCL-SPION allowed detection of tumors by MR imaging and at the same time delivery of sufficient amounts of anticancer drugs that in turn were released from the nanoparticles to exhibit anticancer activity. Consequently, Dox@TCL-SPION showed exceptional antitumor effects without any systemic toxicity. The questions of where the tumor is located, whether drugs are properly delivered to the tumor, and what the therapeutic response of the tumor is, could be answered by using simple but smart, drug-loaded superparamagnetic iron oxide nanoparticles. We anticipate that the aforementioned TCL-SPIONs may be utilized in distinct ways to develop combined therapeutic and diagnostic modalities by incorporating other drugs such as siRNA and small molecular anticancer drugs.

Received: February 21, 2008
Revised: May 9, 2008
Published online: June 12, 2008

Keywords: antitumor agents · drug delivery · imaging agents · nanotechnology

[1] a) X. Qian, et al., *Nat. Biotechnol.* **2008**, *26*, 83 – 90, see the Supporting Information; b) D. Pissuwan, S. M. Valenzuela, M. B. Cortie, *Trends Biotechnol.* **2006**, *24*, 62 – 67; c) K. J. Prashant, H. E.-S. Lvan, A. E.-S. Mostafa, *Nano Today* **2007**, *2*, 18 – 29; d) D. G. Jacob, P. K. Bishnu, R. Z. Eugene, *J. Am. Chem. Soc.* **2007**, *129*, 11653 – 11661; e) L. R. Hirsch, R. J. Stafford, J. A. Bankson, S. R. Sershen, B. Rivera, R. E. Price, J. D. Hazle, N. J. Halas, J. L. West, *Proc. Natl. Acad. Sci. USA* **2003**, *100*, 13549 – 13554; f) J. Kim, et al., *Angew. Chem.* **2006**, *118*, 7918 – 7922; *Angew. Chem. Int. Ed.* **2006**, *45*, 7754 – 7758, see the Supporting Information; g) J. S. Choi, Y. W. Jun, S. I. Yeon, H. C. Kim, J. S. Shin, J. Cheon, *J. Am. Chem. Soc.* **2006**, *128*, 15982 – 15983.

[2] a) A. M. Derfus, A. A. Chen, D. H. Min, F. Ruoslahti, S. N. Bhatia, *Bioconjugate Chem.* **2007**, *18*, 1391 – 1396; b) X. Gao, Y. Cui, R. M. Levenson, L. W. Chung, S. Nie, *Nat. Biotechnol.* **2004**, *22*, 969 – 976; c) A. C. Samia, X. Chen, C. Burda, *J. Am. Chem. Soc.* **2003**, *125*, 15736 – 15737; d) M. E. Akerman, W. C. Chan, P. Laakkonen, S. N. Bhatia, E. Rouslahti, *Proc. Natl. Acad. Sci. USA* **2002**, *99*, 12617 – 12621.

[3] a) J. H. Lee, Y. W. Jun, S. I. Yeon, J. S. Shin, J. Cheon, *Angew. Chem.* **2006**, *118*, 8340 – 8342; *Angew. Chem. Int. Ed.* **2006**, *45*, 8160 – 8162; b) J. H. Lee, et al., *Nat. Med.* **2007**, *13*, 95 – 99, see the Supporting Information; c) M. P. Ana, et al., *J. Natl. Cancer Inst.* **2007**, 99, 53 – 63, see the Supporting Information; d) Z. Medarova, W. Pham, C. Farrar, V. Petkova, A. Moore, *Nat. Med.* **2007**, *13*, 372 – 377; e) N. Nasongkla, et al., *Nano Lett.* **2006**, *6*, 2427 – 2430, see the Supporting Information; f) J. Zhang, R. D. Misra, *Acta Biomater.* **2007**, *3*, 838 – 850; g) G. R. Reddy, et al., *Clin. Cancer Res.* **2006**, *12*, 6677 – 6686, see the Supporting Information.

[4] a) M. Arruebo, R. Fernández-Pacheco, M. R. Ibarra, J. Santamaría, *Nano Today* **2007**, *2*, 22 – 32; b) A. M. Derfus, G. von Maltzahn, T. J. Harris, T Duza, K. S. Vecchio, E. Ruoslahti, S. N. Bhatia, *Adv. Mater.* **2007**, *19*, 3932 – 3936; c) N. Kohler, C. Sun, A. Fichtenholtz, J. Gunn, C. Fang, M. Zhang, *Small* **2006**, *2*, 785 – 792; d) C. Alexiou, et al., *Eur. Biophys. J.* **2006**, *35*, 446 – 450, see the Supporting Information; e) T. K. Jain, M. A. Morales, S. K. Sahoo, D. L. Leslie-Pelecky, V. Labhasetwar, *Mol. Pharmacol.* **2005**, *2*, 194 – 205; f) X. Wang, et al., *J. Biomed. Mater. Res. Part A* **2007**, *80*, 852 – 860, see the Supporting Information.

[5] J. Yang, C. H. Lee, H. J. Ko, J. S. Suh, H. G. Yoon, K. Lee, Y. M. Huh, S. Haam, *Angew. Chem.* **2007**, *119*, 8992 – 8995; *Angew. Chem. Int. Ed.* **2007**, *46*, 8836 – 8839.

[6] a) R. Weissleder, D. D. Stark, B. L. Engelstad, B. R. Bacon, C. C. Compton, D. L. White, P. Jacobs, J. Lewis, *AJR Am. J. Roentgenol.* **1989**, *152*, 167 – 173; b) P. Bourrinet, H. H. Bengele, B. Bonnemain, A. Dencausse, J. M. Idee, P. M. Jacobs, J. M. Lewis, *Invest. Radiol.* **2006**, *41*, 313 – 324.

[7] a) A. S. Lübbe, et al., *Cancer. Res.* **1996**, *56*, 4686 – 4693, see the Supporting Information; b) C. Alexiou, W. Arnold, R. J. Klein, F. G. Parak, P. Hulin, C. Bergemann, W. Erhardt, S. Wagenpfeil, A. S. Lübbe, *Cancer Res.* **2000**, *60*, 6641 – 6648.

[8] H. Lee, E. Lee, D. K. Kim, N. K. Jang, Y. Y. Jeong, S. Jon, *J. Am. Chem. Soc.* **2006**, *128*, 7383 – 7389.

[9] H. Lee, M. K. Yu, S. Park, S. Moon, J. J. Min, Y. Y. Jeong, H. W. Kang, S. Jon, *J. Am. Chem. Soc.* **2007**, *129*, 12739 – 12745.

[10] a) Y. Matsumura, H. Maeda, *Cancer Res.* **1986**, *46*, 6387 – 6392; b) L. Brannon-Peppas, J. O. Blanchette, *Adv. Drug Delivery Rev.***2004**, *56*, 1649 – 1659; c) D. Peer, J. M. Karp, S. Hong, O. C. Farokhzad, R. Margalit, R. Langer, *Nat. Biotechnol.* **2007**, *25*, 751 – 760.

[11] a) Z. Liu, X. Sun, N. Nakayama-Ratchford, H. Dai, *ACS Nano* **2007**, *1*, 50 – 56; b) H. Ali-Boucetta, K. T. Al-Jamal, D. McCarthy, M. Prato, A. Bianco, K. Kostarelos, *Chem. Commun.* **2008**, 459 – 461.

[12] a) V. Bagalkot, O. C. Farokhzad, R. Langer, S Jon, *Angew. Chem.* **2006**, *118*, 8329 – 8332; *Angew. Chem. Int. Ed.* **2006**, *45*, 8149 – 8152; b) V. Bagalkot, L. Zhang, E. Levy-Nissenbaum, S. Jon, P. W. Kantoff, R. Langer, O. C. Farokhzad, *Nano Lett.* **2007**, *7*, 3065 – 3070.

[13] a) B. Dubertret, M. Calame, A. J. Libchaber, *Nat. Biotechnol.* **2001**, *19*, 365 – 370; b) L. Josephson, M. F. Kircher, U. Mahmood, Y. Tang, R. Weissleder, *Bioconjugate Chem.* **2002**, *13*, 554 – 560; c) T. R. Sathe, A. Agrawal, S. Nie, *Anal. Chem.* **2006**, *78*, 5627 – 5632.

[14] S. M. Moghimi, A. C. Hunter, J. C. Murray, *Pharm. Rev.* **2001**, *53*, 283 – 318.

[15] a) P. A. Harris, J. F. Gross, *Cancer Chemother. Rep.* **1975**, *59*, 819 – 825; b) S. Gibaud, J. P. Andreux, C. Weingarten, M. Renard, P. Couvreur, *Eur. J. Cancer Part A* **1994**, *30*, 820 – 826.

